

# An Enhanced Polar-Domain Dictionary Design for Elevated BSs in Near-Field U-MIMO

L. Antonelli, A. A. D’Amico, L. Sanguinetti

Department of Information Engineering, University of Pisa, Pisa, Italy

National Inter-University Consortium for Telecommunications (CNIT), Parma, Italy

**Abstract**—Near-field Ultra-massive MIMO (U-MIMO) communications require carefully optimized sampling grids in both angular and distance domains. However, most existing grid design methods neglect the influence of base station height, assuming instead that the base station is positioned at ground level—a simplification that rarely reflects real-world deployments. To overcome this limitation, we propose a generalized grid design framework that accommodates arbitrary base station locations. Unlike conventional correlation-based approaches, our method optimizes the grid based on the minimization of the optimal normalized mean squared error, leading to more accurate channel representation. We evaluate the performance of a hybrid U-MIMO system operating at sub-THz frequencies, considering the polar simultaneous orthogonal matching pursuit (P-SOMP) algorithm for channel estimation. Analytical and numerical results show that the proposed design enhances both channel estimation accuracy and spectral efficiency compared to existing alternatives.

**Index Terms**—Near-field channel estimation, polar-domain dictionary design, ultra-massive MIMO, sub-THz communications, hybrid architecture.

## I. INTRODUCTION AND MOTIVATION

U-MIMO in the sub-THz band exploits the very short wavelengths to fit a large number of antenna elements into a compact area, which enables significant gains in beam focusing and spatial multiplexing [1]. This is envisioned as a key technology to meet the high traffic demands of wireless communications [2]–[4]. However, in an all-digital architecture, where each antenna is paired with a dedicated radio frequency (RF) chain, this approach would be prohibitively power-intensive, demanding the use of hybrid architectures, where the number of RF chains is limited [5].

In contrast to sub-6 GHz communications, where user equipments (UEs) are typically in the far field of the base station (BS) array and orthogonal codebooks based on discrete Fourier transform matrices are effective, sub-THz frequencies place UEs in the radiating near field [6]. This shift requires the development of near-field codebooks, where the range domain becomes crucial due to the limited beamforming depth, introducing added complexity that goes beyond the angular considerations typical of far-field scenarios [7]. Accordingly, near-field codebooks are built sampling both the angular and range domains, resulting in a larger structure. Therefore, new channel estimation algorithms with overheads independent of dictionary size have emerged. Among them, the P-SOMP [8] exploits channel sparsity for near-field channel estimation.

Existing codebooks fail to properly account for BS height, as they are typically developed under the assumption that the BS is positioned at ground level, which is almost never

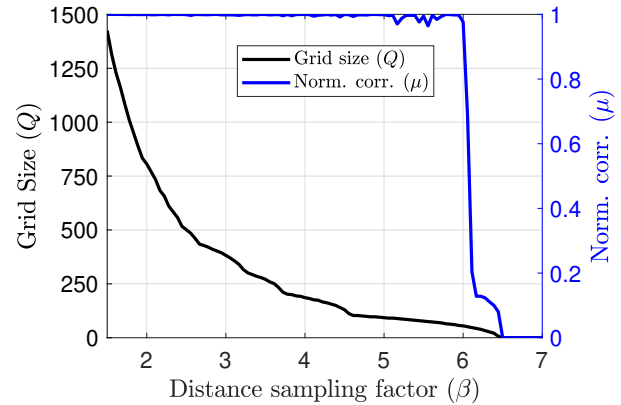


Fig. 1: Normalized correlation  $\mu$  and grid size  $Q$  as a function of the distance sampling factor  $\beta$  with the design in [8].

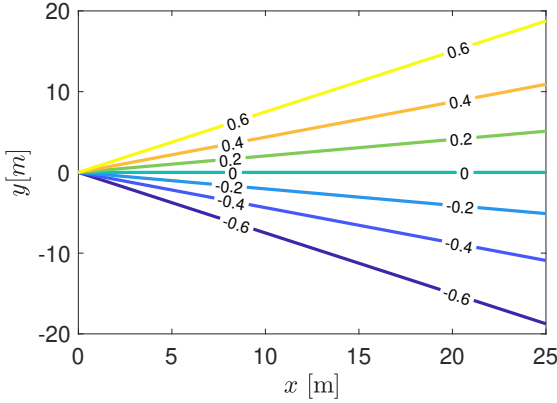
the case. In this paper, we propose a generalized near-field dictionary design criterion for arbitrary BS location above the ground plane (GP) where UEs are displaced.

Additionally, recent designs of polar domain dictionaries for linear and planar arrays focus on the codebook’s column coherence [8], [9] - see Fig. 1. However, since column coherence is not directly related to channel estimation, we use the *optimal NMSE* to improve the codebook’s accuracy. Results show that the proposed codebook outperforms state-of-the art criteria in terms of both channel estimation accuracy and spectral efficiency (SE) regardless of the codebook’s size.

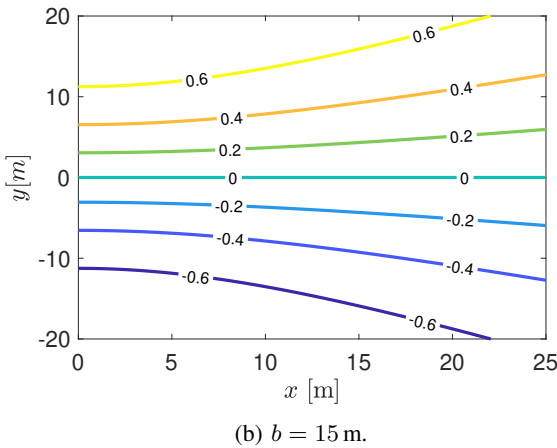
## II. SYSTEM MODEL

We consider the uplink of a U-MIMO system with  $K$  single-antenna active UEs. We assume that the BS is equipped with a uniform linear array (ULA). The number of antennas is  $M$  and the inter-element spacing is  $\delta$ . The array is placed at a height  $b$  above the GP, where UEs are randomly displaced with uniform distribution within a given region-of-interest (RoI). We denote by  $\mathbf{u}_m = [0, i(m)\delta, 0]$  with  $i(m) = (m - \frac{M-1}{2})$  and  $m = 0, 1, \dots, M-1$  the coordinates of antenna  $m$ , and by  $\mathbf{s}_k = (\rho_k \cos \varphi_k, \rho_k \sin \varphi_k, -b)$  with  $\rho_{\min} \leq \rho_k \leq \rho_{\max}$  and  $\varphi_{\min} \leq \varphi_k \leq \varphi_{\max}$  the coordinates of UE  $k$ . Under line-of-sight (LoS) propagation conditions, the electromagnetic channel from UE  $k$  to antenna  $m$  is

$$h_{km} = \sqrt{\xi_m} e^{-j \frac{2\pi}{\lambda} r_{km}} \quad (1)$$



(a)  $b = 0$  m.



(b)  $b = 15$  m.

Fig. 2: Level curves  $\Gamma = g$  with seven different values of  $g$  and BS height  $b = \{0, 15\}$  m.

where  $\xi_{km} \in \mathcal{CN}(0, \sigma_\xi^2)$  with

$$\sigma_\xi^2 = \left( \frac{\lambda}{4\pi r_{km}} \right)^2 \quad (2)$$

accounts for the path loss,  $r_{km} = \|\mathbf{s}_k - \mathbf{u}_m\|$  denotes the Euclidean distance between UE  $k$  and antenna  $m$  at the BS, and  $\lambda$  is the wavelength. We call  $\mathbf{h}_k = [h_{k0}, \dots, h_{k(M-1)}]^T \in \mathbb{C}^M$  the channel vector of UE  $k$ . We consider a hybrid system in which the BS has  $K \leq N_{RF} \ll M$  RF chains. Also, we assume a fully-connected architecture where each antenna is connected to all RF chains [10].

#### A. Channel Estimation

The standard time-frequency division duplex protocol is used [11], where  $\tau_c$  channel uses are available for the uplink channel estimation phase and data transmission. We assume that the  $K$  UEs simultaneously transmit over  $K$  subcarriers, with separation achieved through orthogonal pilot sequences in the frequency-domain. The transmission occurs over  $\tau$  pilot slots in the time domain. Hence, the number of resources used for channel estimation is equal to  $\tau_p = K\tau$ , and the remaining  $\tau_c - \tau_p$  are used for data transmission.

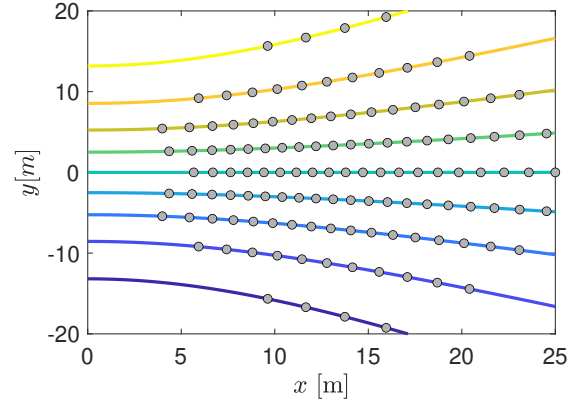


Fig. 3: Example of the proposed grid construction with grid size  $Q = 135$ , number of level curves  $N_\Gamma = 9$  and distance sampling factor  $\beta = 0.57$ .

Signals at different antennas are combined by means of analogue combiners  $\mathbf{a}_{i,r} \in \mathbb{C}^M$  for  $i = 1, \dots, \tau$  and  $r = 1, \dots, N_{RF}$ , whose entries are randomly selected in  $\{\pm 1/\sqrt{M}\}$  with equal probabilities, where the double-subscript notation indicates that different combiners in different time slots and different RF chains may be used. After straightforward computations, the overall pilot signal during the channel estimation phase for each UE can be written as

$$\mathbf{y} = \sqrt{p} \mathbf{K} \mathbf{A} \mathbf{h} + \mathbf{n} \quad (3)$$

where  $p$  is the UE transmit power,  $\mathbf{A} = [\mathbf{A}_1 \dots \mathbf{A}_\tau]^T$  and  $\mathbf{n} = [\mathbf{n}_1^T \dots \mathbf{n}_\tau^T]^T$  where  $\mathbf{A}_i = [\mathbf{a}_{i,1}, \dots, \mathbf{a}_{i,N_{RF}}] \in \mathbb{C}^{M \times N_{RF}}$  is the analog combining matrix for the  $i$ th slot, and  $\mathbf{n}_i \in \mathcal{CN}(\mathbf{0}, \sigma^2 K \mathbf{A}_i^T \mathbf{A}_i^*)$  collects the noise.

We use the P-SOMP algorithm, introduced in [8], to estimate the channel by using the observation vectors in (3). It is based on the polar-domain representation  $\mathbf{h}^P$  of the channel  $\mathbf{h}$ , i.e.,  $\mathbf{h} = \mathbf{W} \mathbf{h}^P$  given in [8, eq. (8)], where  $\mathbf{W} \in \mathbb{C}^{M \times Q}$  is a suitable *dictionary*. More precisely, the  $Q$  columns of  $\mathbf{W}$  are the array steering vectors  $\mathbf{w}(\theta, \varphi, \rho)$  [8, eq. (7)] computed over a discrete grid  $\mathbf{G}$  of  $(\theta, \varphi, \rho)$  values. Accordingly, they depend on the geometry of the array. A good design of  $\mathbf{G}$  is essential for the operation of P-SOMP.

#### B. Review of the Dictionary Design from [8]

A possible grid design for a ULA with  $M$  antennas, lying on the ground plane ( $b = 0$ ), was presented in [8]. Particularly, [8] leads to a sampling of the angular domain with  $M$  points such that  $\Phi = \sin \varphi$  is computed over a uniform grid as

$$\Phi = \frac{2m - M + 1}{M} \quad m = 0, 1, \dots, M - 1. \quad (4)$$

For each angle  $\varphi$  compatible with (4), the distance is non-uniformly sampled as follows [8, Eq. (15)]

$$\rho_n = \frac{Z}{n} \quad n = 0, 1, 2, \dots \quad (5)$$

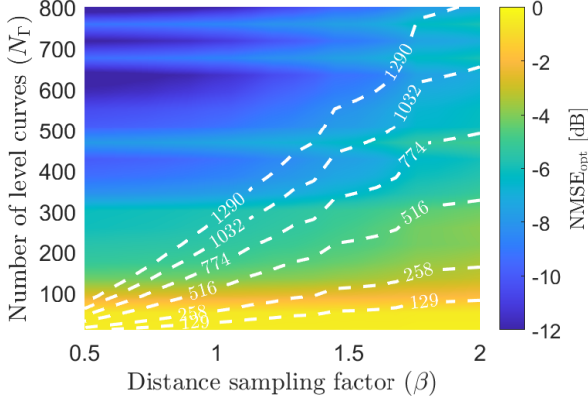


Fig. 4: Proposed design with BS height  $b = 15$  m.

where

$$Z = \frac{1}{2\lambda} \left( \frac{M\delta}{\beta} \right)^2 (1 - \Phi^2) \quad (6)$$

and  $\beta$  is a design parameter [8]. In [8],  $\beta$  is designed by considering the maximum correlation between columns of the dictionary  $\mathbf{W}$ , defined as

$$\mu = \max_{i \neq j} \{ |\mathbf{w}_i^H \mathbf{w}_j| \} \quad (7)$$

where  $\mathbf{w}_i$  and  $\mathbf{w}_j$  are two columns of  $\mathbf{W}$ . On one side, the maximum correlation should be made as small as possible for limiting the number of grid points. On the other side, it cannot be too small because this would lead to a very sparse grid  $\mathbf{G}$ , with very few number of points and a reduced estimation accuracy. Fig. 1 shows  $\mu$  (blue line), normalized by the number of antennas  $M$ , and the dictionary size  $Q$  (black line) as a function of  $\beta$  for a ULA. The blue curve is obtained using the exact (spherical) electromagnetic model for the array steering vectors. We see that increasing  $\beta$  results in smaller values of  $\mu$  and in a smaller grid size. Notably, the only grid design parameter in [8] is the distance sampling factor  $\beta$  in (5). Hence, we can choose  $\beta$  to either achieve a given grid size  $Q$  or a given normalized correlation  $\mu$  in (7), but not both.

### III. PROPOSED POLAR DICTIONARY DESIGN

Our design of the grid is based on the same line of reasoning as in [8], but we also take into account the elevation of the array with respect to the GP. Details are reported in the Appendix, where the concept of a *level curve* is introduced. The latter is defined as the set of points in the GP for which

$$\Gamma(R, \varphi) \stackrel{\text{def}}{=} \cos \theta \sin \varphi = \sqrt{1 - \left( \frac{b}{R} \right)^2} \sin \varphi = g \quad (8)$$

where  $g \in [-1, 1]$  is an arbitrary constant, and  $R$  denotes the distance from the center of the BS array. Fig. 2 shows the level curves in (8) for  $g = 0, \pm 0.2, \pm 0.4, \pm 0.6$ , and  $b = 0, 15$  m. When  $b = 0$ , the level curves appear as straight lines; as the BS elevation  $b$  increases, these curves progressively bend, reflecting the growing influence of elevation.

Parameter	Value
Carrier Frequency, $f_c$	300 [GHz]
Bandwidth, $B$	100 [MHz]
Array Aperture, $L$	0.64 [m]
Number of Antennas, $M$	129
Antenna Spacing, $\delta$	$5\lambda$
Minimum UE distance, $\rho_{\min}$	5 [m]
Maximum UE distance, $\rho_{\max}$	25 [m]
Minimum UE azimuth $\varphi_{\min}$	$-\pi/3$ [rad]
Maximum UE azimuth $\varphi_{\max}$	$\pi/3$ [rad]
BS height, $b$	0, 15 [m]

TABLE I: System parameters.

Parameter	Value
Pilot Sequence Length, $\tau_p$	10
Number of RF chains, $N_{RF}$	10
Transmit Power, $p$	15 [dBm]
Thermal Noise Power, $\sigma^2$	-86 [dBm]
Number of UEs, $K$	10
UEs distribution	Uniform in the RoI
Dictionary size, $Q$	$4M, 10M$

TABLE II: Channel estimation parameters.

#### A. Proposed level curves

Level curves are selected such that  $\Gamma(R, \varphi) = \Gamma_k$  with

$$\Gamma_k = \Gamma_{\max} \left( \frac{2k - N_{\Gamma} + 1}{N_{\Gamma}} \right) \quad k = 0, 1, \dots, N_{\Gamma} - 1 \quad (9)$$

where

$$\Gamma_{\max} = \frac{\rho_{\max}}{\sqrt{\rho_{\max}^2 + b^2}} \sin \varphi_{\max} \quad (10)$$

and  $\{\varphi_{\max}, \rho_{\max}\}$  denote the maximum azimuth and radial distance within the RoI, respectively. The condition  $|\Gamma| < \Gamma_{\max}$  ensures that all used level curves pass through the RoI.

Note that the level curves in (9) play the same role as the straight lines in (4). They coincide when the elevation is zero ( $b = 0$ ),  $\varphi_{\max} = \frac{\pi}{2}$  and  $N_{\Gamma} = M$ . Unlike in (4), where the number of level curves  $N_{\Gamma}$  is fixed to  $M$ , we consider  $N_{\Gamma} \geq M$ , thereby introducing  $N_{\Gamma}$  as an additional design parameter. When  $N_{\Gamma} > M$ , more samples than in [8] are considered in the angular domain in spite of the distance domain. We call this *angular domain over-sampling* and discuss its advantages on channel estimation accuracy.

#### B. Proposed distance sampling

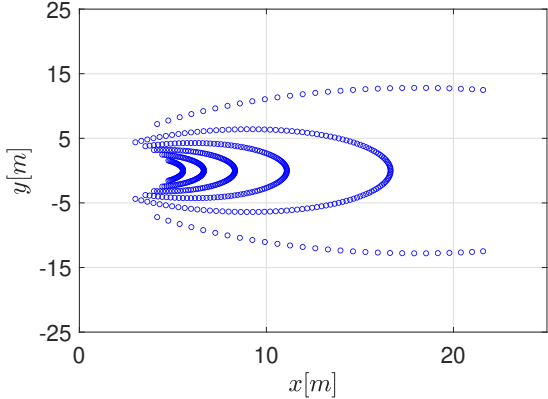
To determine the distance sampling, we select the grid points on each level curve within the RoI. In particular, those belonging to the level curve  $\Gamma(R, \varphi) = \Gamma_k$  are selected so that

$$R_{n,k} = \frac{Z_k R_0}{Z_k + n R_0} \quad n = 0, 1, 2, \dots \quad (11)$$

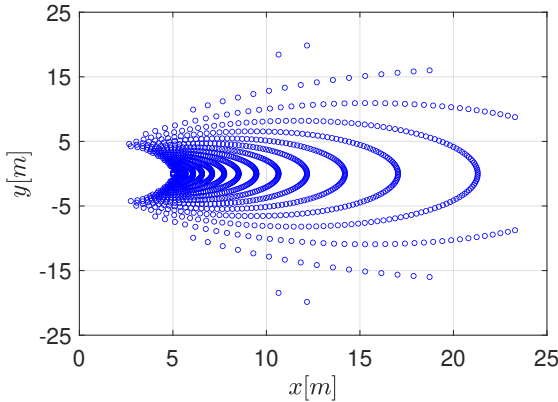
where

$$Z_k = \frac{1}{2\lambda} \left( \frac{M\delta}{\beta} \right)^2 (1 - \Gamma_k^2) \quad (12)$$

$\beta$  is a distance sampling factor, and  $R_0$  is the arbitrary maximum distance considered on each level curve that we



(a)  $\beta = 2.5, Q = 501$ .



(b)  $\beta = 1.56, Q = 1298$ .

Fig. 5: Polar-domain grids obtained using the design in [8] with  $\beta = \{2.5, 1.56\}$  and  $Q = \{501, 1298\}$ , respectively.

set as  $R_0 = \sqrt{\rho_{\max}^2 + b^2}$ . Notice that distances  $R_{n,k}$  in (11) play the same role as radial distances  $\rho_s$  in (5). They coincide when the elevation is zero ( $b = 0$ ),  $\varphi_{\max} = \frac{\pi}{2}$ ,  $N_{\Gamma} = M$  and  $R_0 \rightarrow \infty$ .

#### C. Grid construction

The proposed grid construction can be summarized as follows:

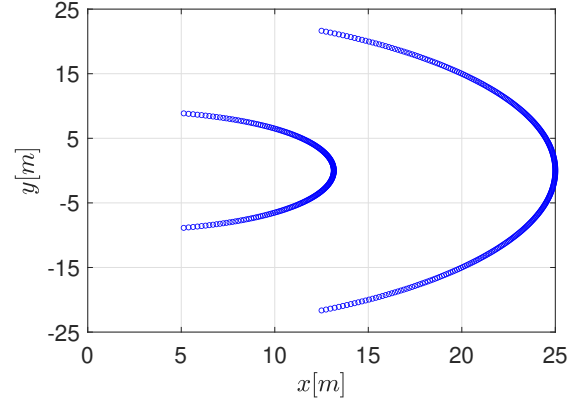
1. Set the grid size  $Q$ .
2. Determine the number of level curves  $N_{\Gamma}$  and the distance sampling factor  $\beta$ .
3. Compute the level curves  $\Gamma(R, \varphi) = \Gamma_k$  from (9).
4. Compute the distances  $R_{n,k}$  using (11).
5. Compute grid points coordinates on each level curve as

$$\left[ \sqrt{R_{n,k}^2(1 - \Gamma_k^2) - b^2}, R_{n,k}\Gamma_k, -b \right]^T. \quad (13)$$

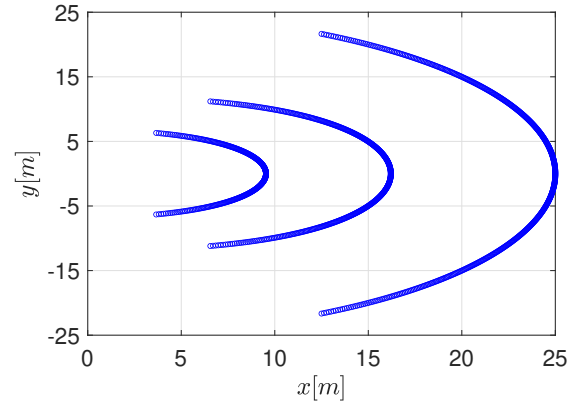
Fig. 3 shows an example of the proposed grid construction with  $Q = 135$ ,  $N_{\Gamma} = 9$  and  $\beta = 0.57$ .

#### D. Grid design

The column coherence in (7) is not directly related to channel estimation. Hence, unlike [8], we design  $N_{\Gamma}$  and  $\beta$



(a)  $N_{\Gamma} = 310, \beta = 1.81, Q = 514$ .



(b)  $N_{\Gamma} = 568, \beta = 1.51, Q = 1290$ .

Fig. 6: Polar-domain grids obtained using the proposed design with  $N_{\Gamma} = \{310, 568\}$ ,  $\beta = \{1.81, 1.51\}$  and  $Q = \{514, 1290\}$ , respectively.

according to the optimal NMSE, defined as

$$\text{NMSE}_{\text{opt}} = 1 - \mathbb{E} \left\{ \min_{\mathbf{g} \in \mathbf{G}} \left[ \frac{|\mathbf{h}^H(\mathbf{g})\mathbf{h}(\mathbf{r})|^2}{\|\mathbf{h}(\mathbf{g})\|^2 \|\mathbf{h}(\mathbf{r})\|^2} \right] \right\} \quad (14)$$

where  $\mathbf{h}(\mathbf{r})$  indicates the channel of the UE located in  $\mathbf{r}$ , and  $\mathbf{h}(\mathbf{g})$  is the channel from the point  $\mathbf{g} \in \mathbf{G}$ . The expectation is computed with respect to the UE's position  $\mathbf{r}$ . Note that  $\text{NMSE}_{\text{opt}}$  can be interpreted as a measure of the average error in approximating the channel at an arbitrary point with the channel at a nearby grid point. From this perspective, lower values of  $\text{NMSE}_{\text{opt}}$  are expected to improve the estimation accuracy for grid-based algorithms, such as the P-SOMP. To understand how to choose  $N_{\Gamma}$  and  $\beta$ , let us consider Fig. 4, which shows the  $\text{NMSE}_{\text{opt}}$  in (14) as a function of both  $\beta$  and  $N_{\Gamma}$ . All other simulation parameters are summarized in Tabs. I and II. It can be observed that, for any given grid size  $q$ , there exist multiple pairs  $(N_{\Gamma}, \beta)$  lying on the level curve corresponding to the constant grid size  $Q = q$  (indicated by white dashed lines), each yielding the desired grid dimension  $q$ . Among these, we choose the pair  $(N_{\Gamma}, \beta)$  that minimizes the  $\text{NMSE}_{\text{opt}}$  in (14).

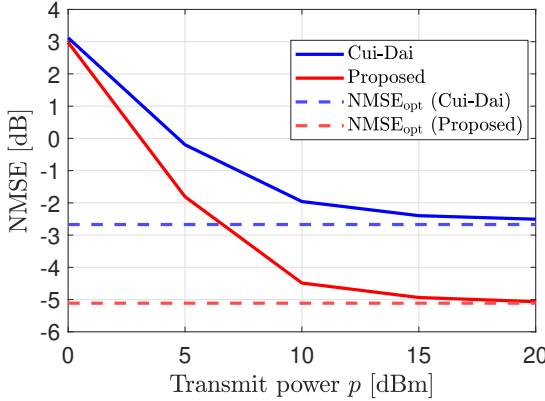


Fig. 7: NMSE and  $\text{NMSE}_{\text{opt}}$  as functions of the transmit power  $p$  in dBm, with grid size  $Q = 4M$ .

#### IV. PERFORMANCE EVALUATION

We now evaluate the P-SOMP algorithm in terms of both channel estimation accuracy and SE. The communication happens at the carrier frequency  $f_c = 300$  GHz, which yields  $\lambda = 1$  mm, over a bandwidth  $B = 100$  MHz. The  $M = 129$  antennas at the BS are spaced by  $\delta = 5\lambda = 5$  mm, which yields an array aperture  $L \approx 0.64$  m. The  $K = 10$  UEs are randomly displaced with uniform distribution within the RoI, which is shaped as the circular sector on the GP with minimum and maximum azimuth angles and radial distances given by  $\varphi_{\max} = -\varphi_{\min} = \frac{\pi}{2}$ ,  $\rho_{\max} = 25$  m and  $\rho_{\min} = 5$  m, respectively. The BS is located at height  $b = 15$  m above the GP. The transmit power of each user is  $p \in [0, 20]$  dBm, and the thermal noise power  $\sigma^2 = -86$  dBm. Eventually, we consider both a smaller and a larger grid size, which are  $Q = \{4M, 10M\}$ , respectively. With these two values of  $Q$ , the design in [8] yields  $\beta = \{2.5, 1.56\}$ , while the proposed method results in  $N_{\Gamma} = \{310, 568\}$  and  $\beta = \{1.8, 1.51\}$ , respectively. Figs. 5 and 6 show the corresponding grids. Notably, despite the grids sharing approximately the same size, the number of level curves is fixed to  $N_{\Gamma} = M$  in [8], while it is  $N_{\Gamma} > M$  in both proposed grids, resulting in a clear angular domain over-sampling. All simulation parameters are summarized in Tables I and II.

We evaluate the channel estimation accuracy in terms of both  $\text{NMSE}_{\text{opt}}$  in (14) and actual NMSE, achieved with the P-SOMP algorithm. Firstly, we consider  $Q = 4M$  and report results as a function of the transmit power  $p$ . Fig. 7 shows that both  $\text{NMSE}_{\text{opt}}$  and NMSE improve up to 3 dB using the proposed design instead of the one in [8]. Additionally, this shows that angular domain oversampling can lead to more precise channel estimation.

The P-SOMP accuracy improves with larger dictionaries. For example, by considering a grid size  $Q = 10M$ , both the dictionary design in [8] and the proposed one yield more accurate channel estimations. Specifically,  $\text{NMSE}_{\text{opt}}$  decreases to  $-5$  dB and  $-8.7$  dB, while the actual NMSE improves to  $-4.2$  dB and  $-7.7$  dB, respectively. However, this

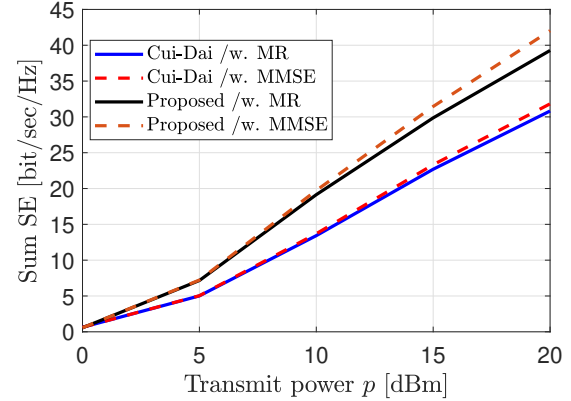


Fig. 8: Sum SE as a function of the power  $p$  with  $K = 10$  UEs and grid size  $Q = 4M$ . Both MR and MMSE combiners are considered.

comes at the price of higher computational complexity of the P-SOMP, which grows linearly with  $Q$  [8].

We now evaluate the achievable sum uplink SE with both maximum ratio (MR) and minimum mean square error (MMSE) combining schemes. This is obtained with the well-known use-and-then-forget bound [11, Sec. 4.2]. Fig. 8 reports the sum SE as a function of  $p$  with  $Q = 4M$ . We see that SE is higher with the proposed design across the whole considered power range. For example, SE approximately improves by 6 bit/sec/Hz for  $p \geq 10$  dBm. The gain on SE increases up to 8 bit/sec/Hz with  $Q = 10M$ .

#### V. CONCLUSIONS

We introduced a novel dictionary design that extends the traditional correlation-based criterion—commonly applied under far-field assumptions—by explicitly accounting for the BS height. Unlike existing approaches, which typically assume the BS is located at ground level, our design generalizes the grid construction to accommodate elevated BS deployments. Furthermore, the grid is dimensioned based on the minimization of the optimal NMSE, rather than the conventional correlation-based metric, enabling a more accurate representation of channel characteristics. The proposed grid is integrated into a hybrid U-MIMO system operating at 300 GHz, employing the P-SOMP algorithm [8] for channel estimation. Simulation results demonstrate that our design consistently outperforms existing grid strategies in terms of both channel estimation accuracy and SE.

#### APPENDIX

We begin with the spherical coordinates of the generic grid point  $\mathbf{p}$ , given by

$$\mathbf{p} = [R \cos \theta \cos \varphi, R \cos \theta \sin \varphi, -b]^T \quad (15)$$

where

$$\cos \theta = \sqrt{1 - \left(\frac{b}{R}\right)^2}. \quad (16)$$

The second-order (i.e., parabolic) approximation of the distance  $r_m = \|\mathbf{p} - \mathbf{u}_m\|$  is given by:

$$r_m \approx -\delta (\cos \theta \sin \varphi) i(m) + \frac{\delta^2}{2R} (1 - \cos^2 \theta \sin^2 \varphi) i^2(m). \quad (17)$$

The associated steering vector can be written as

$$\mathbf{s}(R, \varphi, b) = \left[ e^{j\frac{2\pi}{\lambda} \|\mathbf{p} - \mathbf{u}_0\|}, \dots, e^{j\frac{2\pi}{\lambda} \|\mathbf{p} - \mathbf{u}_{M-1}\|} \right]^\top. \quad (18)$$

Now, let us consider two grid points  $\mathbf{p}$  and  $\mathbf{q}$  with coordinates

$$\mathbf{p} = [R_p \cos \theta_p \cos \varphi_p, R_p \cos \theta_p \sin \varphi_p, -b]^T, \quad (19)$$

$$\mathbf{q} = [R_q \cos \theta_q \cos \varphi_q, R_q \cos \theta_q \sin \varphi_q, -b]^T. \quad (20)$$

Based on (17), the modulus of the correlation between the corresponding steering vectors (after straightforward computations) can be approximated as [8, eq. (9)]:

$$f(\varphi_p, \varphi_q, R_p, R_q) \approx \left| \frac{1}{M} \sum_{m=-(M-1)/2}^{(M-1)/2} e^{j(Am + Bm^2)} \right| \quad (21)$$

where

$$A = \frac{2\pi\delta}{\lambda} (\Gamma_q - \Gamma_p) \quad (22)$$

$$B = \frac{\pi\delta^2}{\lambda} \left[ \frac{1}{R_p} (1 - \Gamma_p^2) - \frac{1}{R_q} (1 - \Gamma_q^2) \right] \quad (23)$$

with

$$\Gamma_i = \cos \theta_i \sin \varphi_i = \sqrt{1 - \left( \frac{b}{R_i} \right)^2} \sin \varphi_i \quad i = p, q \quad (24)$$

Now, assume that the two points  $\mathbf{p}$  and  $\mathbf{q}$  lie on the same level curve, i.e.,  $\Gamma_p = \Gamma_q = g$ . In this case, equations (22) and (23) reduce to

$$A = 0 \quad B = \frac{\pi\delta^2}{\lambda} (1 - g^2) \left( \frac{1}{R_p} - \frac{1}{R_q} \right) \quad (25)$$

Accordingly, the correlation  $f(\varphi_p, \varphi_q, R_p, R_q)$  in (21) becomes

$$f(\varphi_p, \varphi_q, R_p, R_q) = \left| \frac{1}{M} \sum_{m=-(M-1)/2}^{(M-1)/2} e^{jBm^2} \right| \quad (26)$$

which can be further approximated as in [8, Eq. (12)]:

$$f(\varphi_p, \varphi_q, R_p, R_q) \approx |G(\beta)| = \left| \frac{C(\beta) + jS(\beta)}{\beta} \right| \quad (27)$$

where  $C(\beta)$  and  $S(\beta)$  are the cosine and sine Fresnel integral functions [12], respectively, and

$$\beta^2 = \frac{M^2 \delta^2 (1 - g^2)}{2\lambda} \left| \frac{1}{R_p} - \frac{1}{R_q} \right|. \quad (28)$$

Equation (27) shows that, by varying  $\beta$ , we may control the correlation between the channels (actually, the steering vectors) in  $\mathbf{p}$  and  $\mathbf{q}$ . Additionally, equation (28) leads to the distance sampling criterion in (11) and (12), where  $R_0$  is an additional design parameter denoting the arbitrary maximum

distance from grid points to the BS on each level curve. Unlike [8], where  $R_0 \rightarrow \infty$ , we consider  $R_0 = \sqrt{\rho_{\max}^2 + b^2}$ , taking into account that our RoI is limited.

In order to construct the grid, we need to fix the number of level curves  $N_\Gamma$  and their values. To this end, observe that the difference  $\Gamma_p - \Gamma_q$  determines the correlation  $f(\varphi_p, \varphi_q, R_p, R_q)$  in the far field, when  $R_p \rightarrow \infty$  and  $R_q \rightarrow \infty$ , as can easily be derived from (21)-(23). Indeed, in this case  $B \rightarrow 0$  and (21) reduces to

$$f(\varphi_p, \varphi_q, R_p, R_q) \approx \left| \frac{\sin \left[ \frac{\pi M \delta}{\lambda} (\Gamma_p - \Gamma_q) \right]}{M \sin \left[ \frac{\pi \delta}{\lambda} (\Gamma_p - \Gamma_q) \right]} \right| \quad (29)$$

This suggests considering values of  $\Gamma$  uniformly spaced in the interval  $(-\Gamma_{\max}, \Gamma_{\max})$ , which leads to the level curves selection criterion in (9).

Once the level curves  $\Gamma(R, \varphi) = \Gamma_k$  and the distances  $R_{n,k}$  on each level curve have been chosen according to (9) and (11), respectively, we compute the spherical coordinates of each grid point in (15) as per (13).

## ACKNOWLEDGMENT

This work has been performed in the framework of the HORIZON-JU-SNS-2022 project TIMES, cofunded by the European Union. Views and opinions expressed are however those of the author(s) only and do not necessarily reflect those of the European Union.

## REFERENCES

- [1] Björnson *et al.*, “Massive MIMO is a reality—what is next?: Five promising research directions for antenna arrays,” *Digital Signal Processing*, vol. 94, 2019.
- [2] C. Castro *et al.*, “Long-range high-speed thz-wireless transmission in the 300 ghz band,” in *Third International Workshop on Mobile Terahertz Systems (IWMTS)*, 2020.
- [3] K. C. Huang and Z. Wang, “Terahertz terabit wireless communication,” *IEEE Microwave Magazine*, vol. 12, no. 4, 2011.
- [4] T. S. Rappaport *et al.*, “Wireless communications and applications above 100 ghz: Opportunities and challenges for 6g and beyond,” *IEEE access*, vol. 7, 2019.
- [5] C. Han, L. Yan, and J. Yuan, “Hybrid beamforming for terahertz wireless communications: Challenges, architectures, and open problems,” *IEEE Wireless Communications*, vol. 28, no. 4, 2021.
- [6] G. Bacci, L. Sanguinetti, and E. Björnson, “Spherical wavefronts improve MU-MIMO spectral efficiency when using electrically large arrays,” *IEEE Wireless Communications Letters*, vol. 12, no. 7, 2023.
- [7] E. Björnson, Ö. T. Demir, and L. Sanguinetti, “A primer on near-field beamforming for arrays and reconfigurable intelligent surfaces,” in *IEEE Asilomar*, 2021.
- [8] M. Cui and L. Dai, “Channel estimation for extremely large-scale mimo: Far-field or near-field?” *IEEE Transactions on Communications*, vol. 70, no. 4, pp. 2663–2677, 2022.
- [9] Ö. T. Demir and E. Björnson, “A new polar-domain dictionary design for the near-field region of extremely large aperture arrays,” in *Proceedings of IEEE CAMSAP*, 2023.
- [10] A. F. Molisch *et al.*, “Hybrid beamforming for massive mimo: A survey,” *IEEE Communications Magazine*, vol. 55, no. 9, pp. 134–141, 2017.
- [11] E. Björnson, J. Hoydis, and L. Sanguinetti, “Massive MIMO networks: Spectral, energy, and hardware efficiency,” *Foundations and Trends® in Signal Processing*, vol. 11, no. 3-4, pp. 154–655, 2017.
- [12] J. Sherman, “Properties of focused apertures in the fresnel region,” *IRE Transactions on Antennas and Propagation*, vol. 10, no. 4, pp. 399–408, 1962.